LANGMUIR
Cite This: Langmuir 2019, 35, 3383−3390
Article
pubs.acs.org/Langmuir

Tunable Phospholipid Nanopatterns Mediated by Cholesterol with Sub-3 nm Domain Size

Chia-Chun Lee, Chen-Shin Lin, and Shih-Huang Tung*

Institute of Polymer Science and Engineering and Advanced Research Center for Green Materials Science and Technology, National Taiwan University, Taipei 10617, Taiwan

Supporting Information

ABSTRACT: The interactions between phospholipids and cholesterol have been extensively studied in the aqueous systems because of their vital functionalities in the cell membrane. In this study, instead of the self-assembly in water, we explored the microphase-separated structures of phospholipids in bulk and thin films in the absence of solvents and created a series of ordered nanostructures by incorporation of cholesterol into phospholipids. Three zwitterionic two-tailed phospholipids, that is, phosphatidylcholines (PCs), with different numbers of double bonds on the hydrocarbon tails were investigated, including egg PC, 1,2-dioleoyl-*sn*-glycero-3-phosphocholine (DOPC), and 1,2-dipalmitoyl-*sn*-glycero-3-phosphocholine (DPPC). We find that the nanostructures are highly dependent on the conformation of the tails on the PCs, which can be tailored by the number of double bonds on tails and the molar ratio of cholesterol to PC. By changing the molar ratio, egg PC with one double bond organizes into rich microdomains, including lamellae, spheres, and cylinders, whereas DOPC with two double bonds form spheres and cylinders and DPPC with no double bond forms lamellae only. The sizes of the microdomains are less than 3 nm, smaller than those of typical block copolymers. The biomolecule-based nanopatterns developed in this work provide a platform toward future applications of nanotechnology and biotechnology.

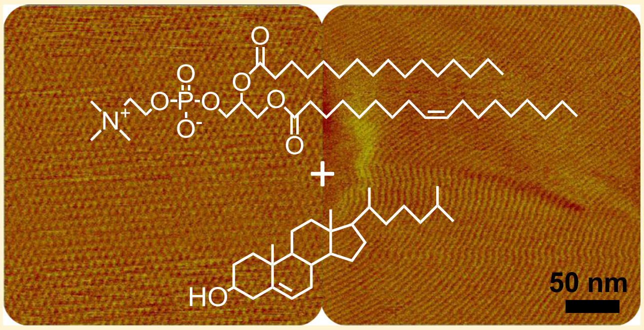

■ INTRODUCTION

Phospholipids consisting of a hydrophilic headgroup and hydrophobic tails are the major lipids of cell membranes responsible for membrane transport and mediation of the membrane-embedded species. Because of the crucial role of phospholipids in cell physiology, the self-assembly behaviors of phospholipids in water have long held scientific interest and the development in this field has inspired versatile applications, such as drug and gene delivery or templating synthesis.[1] In addition to aqueous solutions, the reverse micellization of phospholipids in low-polar organic solvents, such as alkanes, has also been systematically studied.[2−6] In contrast, although the pioneering works have shown that lipids in bulk state or thin films form diverse structures that are promising for biotechnological applications, such as RNA carriers,[7−9] the investigations on the nanostructures of phospholipids in dried bulk or thin films remain relatively rare, especially lack of a deep understanding of the formation mechanisms for the nanostructures other than the bilayer commonly seen for phospholipids.[10−15] Analogous to block copolymers with incompatible chains well-known for their fascinating ordered phase-separated nanostructures, phospholipids with incompatible hydrophilic headgroups and hydrophobic tails are able to segregate into nanopatterns in the absence of solvents.

The macroscopic properties of materials are closely related to the length scales of the structures in the materials. The feature size of the nanostructures in block copolymers is typically in the scale of ∼10 to 10^2 nm. Much effort has been made to pursue sub-10 nm domains or even smaller size to meet the demands of more sophisticated processing or to push the nanotechnology forward. However, achieving a smaller size has never been a simple task because the minimum possible domain size of block copolymers is determined by both the degree of polymerization N and the interaction parameter χ, and reducing the molecular weight to reach a smaller size may cause the product χN to be lower than a critical value for a block copolymer to segregate.[16,17] Therefore, the creation of small domains requires a low N value and a very high χ parameter, and only a few of such copolymers have been successfully synthesized.[18−22] Recently, in addition to low-molecular-weight block copolymers, the strategies for the molecular design of self-assembling liquid-crystalline small molecules[23,24] and POSS/C_{60}-based giant surfactants[25,26] have been reported to produce nanostructures with sub-10 nm feature sizes. However, the precise synthesis of such materials in large quantity remains challenging.

A variety of phospholipids can be extracted from nature sources, such as eggs and soy beans, or can be synthesized for

Received: September 10, 2018
Revised: January 29, 2019
Published: February 8, 2019

DOI: 10.1021/acs.langmuir.8b03075
Langmuir 2019, 35, 3383−3390

specific purposes. Phosphatidylcholines (PCs) are a class of zwitterionic phospholipids, bearing hydrocarbon tails and a negatively charged phosphate coupled with a positively charged choline on headgroups. The molecular weight of the same kind of PC is rather uniform, and the hydrophilic headgroups and hydrophobic tails are highly incompatible. In this study, we show that PCs are capable of forming dense arrays of phase-separated domains, including lamellae, spheres, and cylinders, with a sub-3 nm size because of their low molecular weight. For block copolymers, the nanostructures are determined by the volume fraction of each block that can be tuned by molecular weights.[17] For PCs, we found that the nanostructures are determined by the conformation and flexibility of the hydrophobic tails, and we adopted the approaches other than molecular-weight control to tailor the shapes of the microdomains of PCs. First, PCs with different numbers of double bonds on tails were used in this work, including egg PC, 1,2-dioleoyl-*sn*-glycero-3-phosphocholine (DOPC), and 1,2-dipalmitoyl-*sn*-glycero-3-phosphocholine (DPPC), as shown in Figure 1. The double bond on the

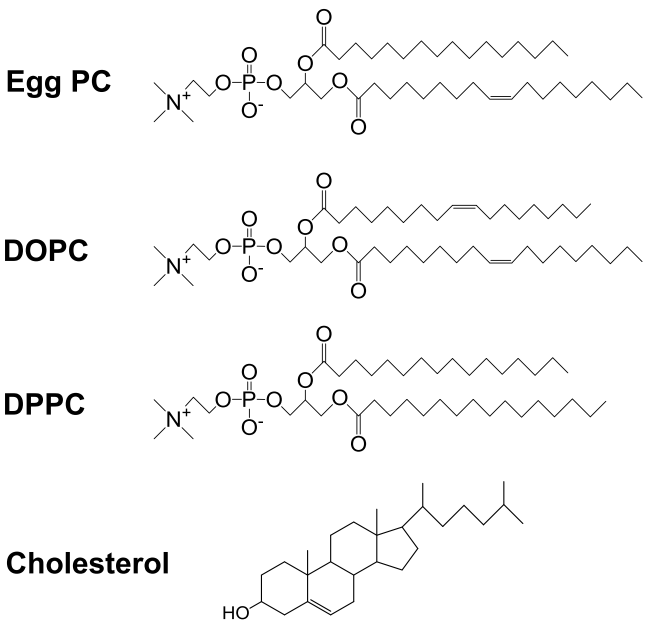

Figure 1. Molecular structures of PCs and cholesterol used in this study.

tails causes a tail configuration unfavorable for close packing, and thus, the coiled flexible chains result in high-curvature microdomains instead of lamellae, like spheres and cylinders. Second, cholesterol, also a lipid in the cell membrane, was incorporated into PCs, which can alter the conformation of PC tails, and therefore, the nanostructures can be tuned in a controlled manner.

Cholesterol composes about 20−30% of the total lipids in animal cell membranes, essential to maintain structural integrity and to regulate the fluidity of the membrane.[27] In the cell membrane, the hydroxyl group on cholesterol interacts with the headgroups of phospholipids through hydrogen bonding and the hydrophobic moieties are buried in the tail area. Previous literature studies have shown that cholesterol, due to its hydrophobic rigid steroid rings (Figure 1), can reduce the flexibility of phospholipid tails and inhibit the chain motion in the fluid state of bilayers, known as ordering or condensing effect.[28−31] On the other hand, when the phospholipids are in the gel phase, that is, tails are frozen and crystallize below chain melting temperature, the insertion of cholesterol hinders the close packing of the tails. Therefore, the flexibility and the mobility of the tails are enhanced instead.[32,33] We utilized the interactions between PCs and cholesterol in fluid and frozen state to manipulate the nanostructures formed by their mixtures in the dried state. The samples were cast from the solutions of the mixtures in a low-polar organic solvent, that is, cyclohexane, where the PCs self-assemble into reverse spherical micelles.[5] Ordered lamellae, spheres in face-centered cubic (fcc) stacking, and cylinders in hexagonal close packing (HEX) with sub-3 nm size can be obtained through the use of different PCs as well as the adjustment of molar ratio of the mixtures. The biomolecule-based nanopatterns are expected to find versatile applications, such as sensing, templating used to guide the self-assembly or the synthesis of nanomaterials, and the carriers for drug or gene delivery.

■ EXPERIMENTAL SECTION

Materials. L-α-PC (egg PC, >99% purity), DOPC (>99%), and DPPC (>99%) were purchased from Avanti Polar Lipids, Inc. Cholesterol (≥99%) was purchased from Sigma-Aldrich. The purities of the solvents used in this work, including cyclohexane and anhydrous methanol, were higher than 99.5%. All chemicals were used as received.

Sample Preparation. PCs and cholesterol were dissolved in anhydrous methanol to form 10 mM stock solutions. The molar ratio of cholesterol to PC was tuned by mixing different amounts of the stock solutions. After mixing, methanol was removed in a vacuum oven at 55 °C for 48 h. This step also ensures the residual water in the PC headgroups as low as possible at a 0.9:1 molar ratio to PC in the dried samples.[5] The dried cakes were then dissolved in cyclohexane at a PC concentration of 10 mM. The dried bulk samples were collected in beakers by removing cyclohexane in a vacuum oven for 48 h at room temperature. For the preparation of thin films, solutions were spun-cast onto silicon wafers to form films with a thickness of ∼40−60 nm, determined by a Filmetrics F20 interferometer. The samples were stored in vacuumed chambers before characterization to avoid moisture that would affect the phase-separated structures.

X-ray Scattering. Transmission-mode small-angle X-ray scattering (SAXS) was conducted on beamline B23A1 in the National Synchrotron Radiation Research Center (NSRRC), Taiwan.[34] The one-dimensional scattering intensity profiles were obtained by circularly averaging the two-dimensional (2-D) patterns collected on a Pilatus 1 M detector with an area of 169 mm × 179 mm (981 pixels × 1043 pixels) and reported as the plots of scattering intensity I versus the scattering vector q, where $q = (4\pi/\lambda)\sin(\theta/2)$ and θ is the scattering angle. Grazing-incidence SAXS (GISAXS) for thin films was carried out on the same beamline. The incident angle was 0.2°. The scattering experiments were conducted at 25 °C without intended humidity control, and the scattering angle was calibrated using silver behenate as the standard.

Atomic Force Microscopy. Atomic force microscopy (AFM) images were taken under ambient conditions in tapping mode on a MultiMode AFM system with a Nanoscope 3D controller (Digital Instruments/Veeco Metrology). Silicon cantilevers (PPP-NCHR-50 from Nanosensor) with a spring constant of 25−80 N/m and the resonant frequency of ∼330 kHz were used.

Fourier Transform Infrared Spectroscopy. Fourier transform infrared spectroscopy (FTIR) spectra were recorded in transmission mode with a PerkinElmer Spectrum 100 model FTIR spectrometer at room temperature. Solution samples of 50 mM PC with different molar ratios of cholesterol in cyclohexane were loaded into a CaF_2 cell in 0.05 mm thickness and analyzed in the range of wavenumbers from 4000 to 900 cm^{-1}. Each spectrum was collected by an accumulation

DOI: 10.1021/acs.langmuir.8b03075
Langmuir 2019, 35, 3383−3390

of 8 scans at 1 cm^{-1} resolution. For the measurements of solid samples, the mixed solutions were cast onto CaF_2 pellets, and the samples were dried in a vacuum oven.

Differential Scanning Calorimetry. Differential scanning calorimetry (DSC) thermograms were collected on a TA Instruments DSC Q20 under nitrogen atmosphere. Dried samples of 2−3 mg were encapsulated in sealed aluminum pans and heated at a rate of 10 °C/min. Indium was used as the standard for temperature calibration.

■ RESULTS AND DISCUSSION

The microphase-separated structures of the three PCs, egg PC, DOPC, and DPPC, induced by cholesterol are summarized in Table 1. Egg PC that mostly bears one double bond on one tail shows abundant structures varying with the molar ratio of cholesterol to PC (x). We thus first discuss the self-assembled behaviors of the egg PC/cholesterol mixtures, followed by the mixtures of DOPC with two unsaturated tails, that is, one double bond on each tail, and DPPC bearing two saturated tails without double bond.

Table 1. Structures of PCs Mixed with Cholesterol at Varying Ratios

x	egg PC	DOPC	DPPC
0	lamella (5.1 nm)[a]	sphere (5.4 nm)	lamella (5.7 nm)
0.1	lamella (4.9 nm)	sphere (5.3 nm)	lamella (5.9 nm)
0.3	lamella (5.0 nm)	sphere (5.3 nm)	lamella (5.7 nm)
0.5	sphere (5.8 nm)	sphere + cylinder	lamella (5.7 nm)
0.7	sphere + cylinder	cylinder (4.2 nm)	lamella (5.7 nm)
0.9	cylinder (4.5 nm)	cylinder (4.1 nm)	lamella (5.7 nm)

[a] d-spacing calculated from the diffraction peak at the lowest q.

Egg PC/Cholesterol Mixtures. Figure 2a shows the SAXS data of egg PC/cholesterol bulk samples with varying x

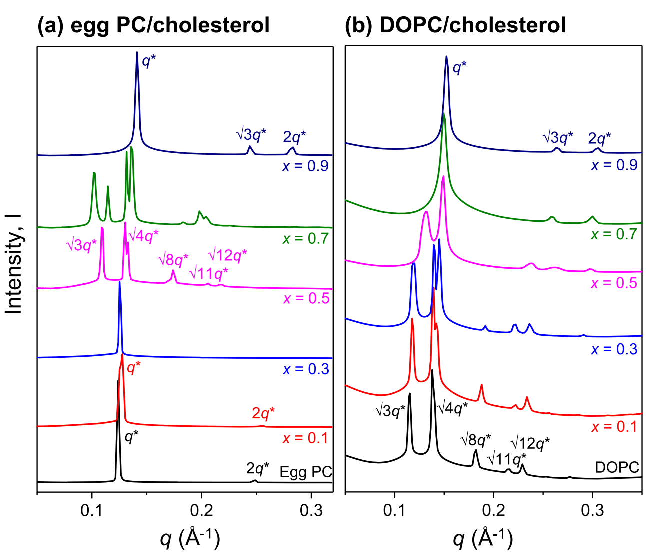

Figure 2. SAXS data of (a) egg PC/cholesterol and (b) DOPC/cholesterol mixtures. x is the molar ratio of cholesterol to PCs. The data were collected at 25 °C.

collected at 25 °C. At $x \leq 0.3$, the q values of the diffraction peaks are at 1:2 ratio and the d-spacing is ∼5 nm. Pure egg PC self-organizes into a lamellar structure, and the amount of cholesterol at $x \leq 0.3$ is insufficient to change the lamellar structure. At $x = 0.5$, the scattering profile changes dramatically. Multiple peaks appear in the order of $\sqrt{3}$, $\sqrt{4}$, $\sqrt{8}$, $\sqrt{11}$, and $\sqrt{12}$, characteristic of the fcc spheres,[35] and the largest d-spacing is 5.8 nm. As x further increases, the structure keeps evolving, and at $x = 0.9$, the q ratio of the peaks becomes 1:$\sqrt{3}$:2 with a d-spacing ∼4.5 nm, which is the diffraction profile caused by HEX cylinders. At $x = 0.7$, the q ratio of the diffraction peaks is not from typical order structures, possibly in the transition state between fcc spheres and HEX cylinders. The SAXS data clearly show the transformation of the original lamellae into fcc and HEX structures upon the incorporation of cholesterol into egg PC. Note that the d-spacings of the ordered structures in this system are about 5 nm and the domain size is expected to be smaller than 3 nm, much smaller than the sizes of the phase-separated microdomains of typical block copolymers.

The AFM phase images of the thin films formed by egg PC/cholesterol mixtures at different x are shown in Figure 3, and

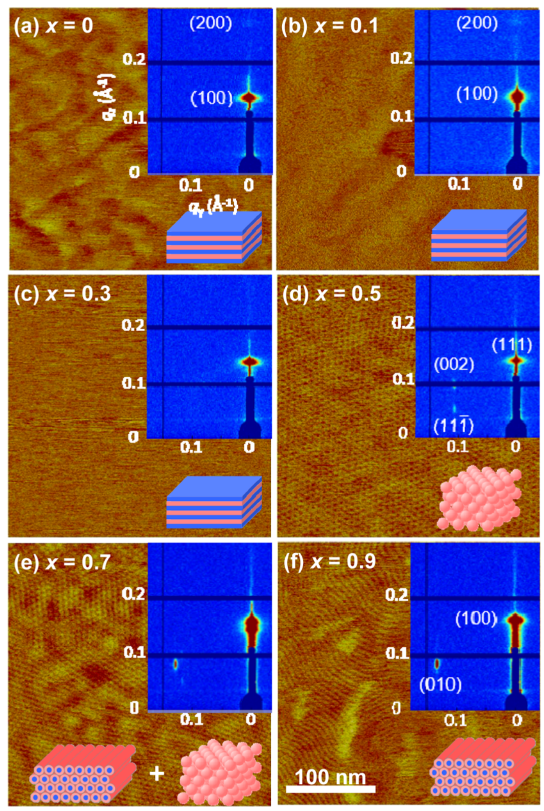

Figure 3. AFM phase images and GISAXS patterns of egg PC/cholesterol thin films at varying x.

the corresponding GISAXS patterns are shown in the insets. At $x = 0$−0.3, the surfaces of the films are featureless and the GISAXS patterns show the diffraction spots along q_z direction with a 1:2 ratio, indicating that the lamellae are parallel to the substrate in the thin films. At $x = 0.5$, a highly ordered array of spheres can be observed on the surface (Figure 3d), and the GISAXS pattern reveals an fcc arrangement of the spheres with (002) and $(11\bar{1})$ characteristic diffraction spots. At $x = 0.9$, a fingerprint-like texture can be seen on the surface (Figure 3f), which is the wandering cylinder parallel to the substrate. The GISAXS pattern confirms the parallel cylinders that pack in a hexagonal manner. A texture that combines spheres and cylinders appear for the thin film at $x = 0.7$ (Figure 3e), consistent with the GISAXS pattern that exhibits both the characteristics of fcc and HEX structures.

DOI: 10.1021/acs.langmuir.8b03075
Langmuir 2019, 35, 3383−3390

The scattering data and AFM phase images have shown that the incorporation of cholesterol can alter the self-assembled structures of egg PC in bulk samples and thin films. FTIR was then used to clarify the interactions between egg PC and cholesterol in solutions and dried films. We first discuss the FTIR data of the solutions. Figure 4 shows the spectra of the

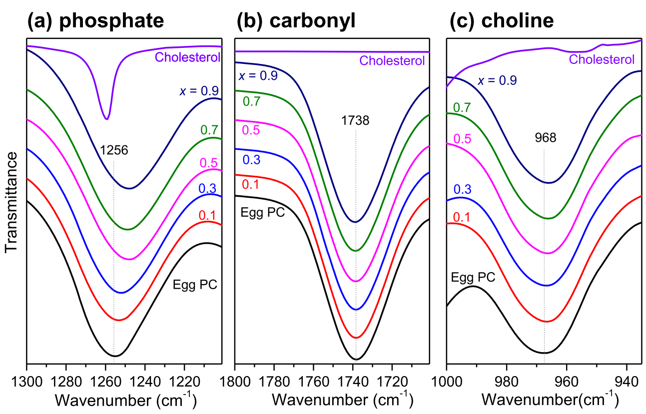

Figure 4. FTIR absorption bands of (a) phosphate, (b) carbonyl, and (c) choline group on egg PC at varying x in cyclohexane at 25 °C.

phosphate (PO_4^-), carbonyl (C=O), and choline (CN-$(CH_3)_3^+$) on egg PC at varying molar ratio x in cyclohexane solutions where egg PC forms reverse micelles.[5] It has been reported that the phosphate of PCs is the primary group that interacts with other polar or ionic molecules.[36,37] In Figure 4a, the absorption band of the phosphate on pure egg PC is found at 1256 cm^{-1}. The band red-shifts to 1248 cm^{-1} as x increases to 0.5 and remains constant until x = 0.9, indicating that the hydroxyl group on cholesterol forms hydrogen bonds with the phosphate and the interaction is saturated at x = 0.5, above which the excess cholesterol molecules prefer to dissolve in cyclohexane instead of interacting with egg PC. The absorption band of carbonyl is not significantly dependent on x, as shown in Figure 4b, and a subtle blue shift to 1739 cm^{-1} at x = 0.7−0.9 from the original 1738 cm^{-1} was detected, which is attributed to the weakening of the carbonyl dipole−diploe interaction upon the insertion of cholesterol that slightly separates egg PC molecules.[36] In the reverse micelles, the positively charged choline should adopt a tilt conformation to associate with the negatively charged phosphate on adjacent egg PC molecule so as to lower interaction energy.[38] In Figure 4c, the absorption band of choline slightly red-shifts from 968 to 966 cm^{-1} with increasing x, indicating a stronger interaction between choline and phosphate when cholesterol is incorporated. This suggests that the insertion of cholesterol affects the molecular conformation of egg PC to allow a packing more favorable to the choline−phosphate interaction.

Figure 5 shows the FTIR spectra of the dried egg PC/cholesterol films. In Figure 5a, the absorption band of the phosphate on pure egg PC is at 1237 cm^{-1}, further red-shifting from those with cholesterol in solutions (1248 cm^{-1}), and the band is not changed upon mixing with cholesterol. Similarly, in Figure 5c, the choline bands are constantly at 969 cm^{-1}, independent of x. This suggests that in dried films, the phosphate and choline groups of egg PC molecules are closely packed and the strong molecular interactions between egg PC are not disturbed by cholesterol. The closely packed egg PC in dried films is confirmed by the change of carbonyl band shown

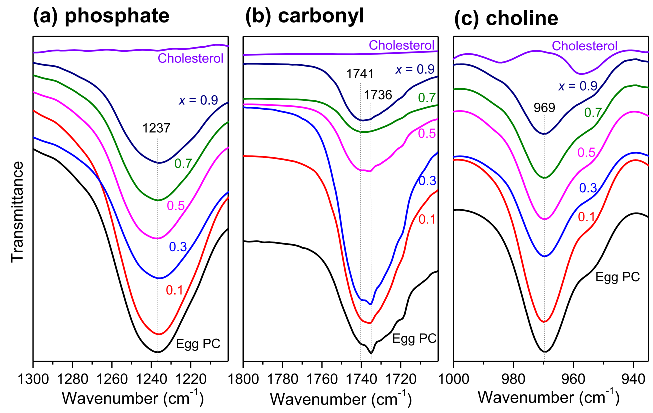

Figure 5. FTIR absorption bands of (a) phosphate, (b) carbonyl, and (c) choline group on egg PC at varying x in dried films at 25 °C.

in Figure 5b, where a red-shifted band at 1736 cm^{-1} compared to that in solutions for pure egg PC (1738 cm^{-1}) can be seen. Unlike the constant phosphate and choline bands, the carbonyl band shows a significant change with x. The sharper band at 1736 cm^{-1} at x below 0.5 is the absorption of carbonyl on the closely packed egg PC in dried films. At $x \geq 0.5$, the sharp band disappears, and instead, a broad band at 1741 cm^{-1} representing a weaker dipole−dipole interaction becomes pronounced, indicating that in the dried thin films, the cholesterol molecules can effectively insert into the tail areas of egg PC and separate the carbonyl groups of adjacent egg PC molecules even though the phosphate and choline groups are unaffected.

The thermal behaviors of the egg PC/cholesterol mixtures were studied by DSC as shown in Figure 6a. The melting peak

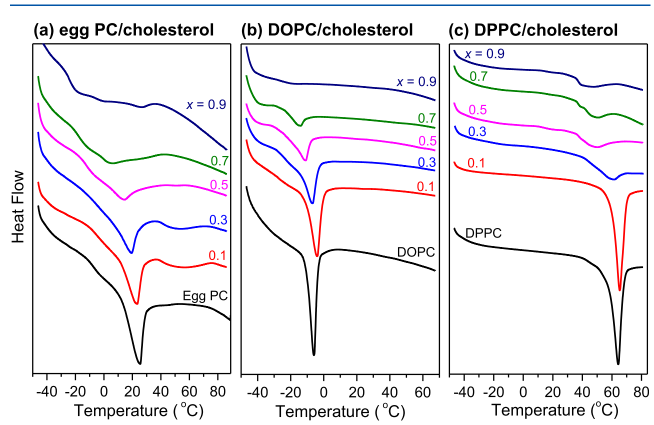

Figure 6. DSC thermograms of (a) egg PC/cholesterol, (b) DOPC/cholesterol, and (c) DPPC/cholesterol mixtures at varying x.

of the pure egg PC is at 25.5 °C. In other words, around room temperature, pure egg PC can maintain the crystalline state where the alkyl tails are extended and closely pack to form a lamellar structure. The melting temperature decreases as x increases, confirming the interference of cholesterol with the packing of egg PC. At x = 0.3, egg PC melts at 19.4 °C, not far below room temperature, and egg PC still tends to form lamellae. Note that for x = 0.1 and 0.3, another broad endothermic signal is observed between 35 and 70 °C, which could be attributed to the dissociation of the hydrogen bonds between egg PC and cholesterol. At x above 0.5, the melting temperature becomes much broader and is below 15 °C,

DOI: 10.1021/acs.langmuir.8b03075
Langmuir 2019, 35, 3383−3390

indicating that at room temperature, the tails on egg PC are more flexible, no longer closely packed. This creates larger effective tail areas and should be correlated with the formation of the spherical and cylindrical domains at x above 0.5.

The plausible mechanism for the formation of the structures varying with x is discussed below and illustrated in Figure 7. At

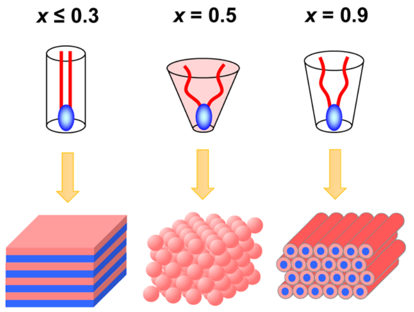

Figure 7. Schematic of the molecular geometry of egg PC at varying x and the resulting nanostructures. At $x \leq 0.3$, the tails of egg PC prefer to straighten and the molecules in cylindrical shape tend to form lamellae. At $x = 0.5$, the fcc spherical domains are retained from the spherical micelles in cyclohexane where the swollen tails cause a conical molecular shape that fits the curvature of a sphere. At $x = 0.9$, a sufficient amount of cholesterol inserts between egg PC to enhance the chain ordering, and the molecular geometry becomes a truncated cone that favors cylindrical domains.

x below 0.3, where the amount of cholesterol is insufficient to significantly affect the assembly of egg PC, the formation of lamellae at room temperature is favorable because the tails of egg PC prefer to straighten and closely pack to lower the molecular interaction energy as well as to adopt a flat interface so as to minimize the interfacial area. At $x = 0.5$, it is rational that the tendency of the tails to form lamellae is decreased because the insertion of cholesterol hinders the close packing of egg PC.[32,33] Structures other than lamella, including spherical and cylindrical domains, can thus form because of the more flexible tails that change the curvature of the interface between the hydrophilic headgroups and the hydrophobic tails. However, the direct transition from lamellar to spherical domains without an intermediate cylindrical phase is intriguing. It has been known that PCs form nearly spherical reverse micelles in low-polar organic solvents because of the swollen tails.[5] We suggest that the spherical domains found in the dried samples at $x = 0.5$ are retained from the spherical micelles in the solutions, which are quickly stacked into the fcc structure and temporarily frozen after evaporation of the solvent. This is confirmed by the fact that the spherical domains slowly evolve into thermodynamically more stable cylindrical domains after 5 days, as shown in Figure S1 of the Supporting Information. At x above 0.7, because a sufficient amount of cholesterol inserts between egg PC to enhance the conformational ordering of the tails in the melt state,[28−31] the mixtures can rapidly organize into the stable HEX cylindrical domains upon solvent evaporation. The schematic of the formation mechanism based on the molecular geometry of egg PC that changes with the tail conformation is shown in Figure 7. Note that we have exhaustively dried both the egg PC and cholesterol prior to use, as described in the Experimental Section. The residual water content is too small to explain the structures as the lyotropic phases of lipids generally found in concentrated aqueous solutions. The results show that cholesterol has a distinct influence on structural changes of egg PC in dried samples. In sum, by incorporation of cholesterol into egg PC, ordered lamellar, spherical, and cylindrical microdomains can be obtained either kinetically or thermodynamically, depending on the molar ratio of cholesterol to egg PC.

DOPC/Cholesterol Mixtures. The major difference between DOPC and egg PC is that both of the two DOPC tails contain one double bond, while most egg PC molecules only have one double bond on one of the tails. The presence of double bonds on alkyl chains lowers the regularity of the chains, which in turn hinders the interchain close packing and allows a more flexible chain conformation. Therefore, it is expected that DOPC inclines to form structures other than lamella in dried samples. Figure 2b shows SAXS profiles of DOPC mixed with cholesterol at different ratios. Indeed, unlike the behavior of egg PC, pure DOPC and the mixture at $x = 0.1$ stack into an fcc structure after solvent evaporates. At x above 0.7, the mixtures form HEX cylinders. Between $x = 0.3$ and 0.5, the mixtures are in the transition states where the fcc spheres gradually transform into HEX cylinders as x increases. The AFM phase images with the insets of corresponding 2-D GISAXS data for DOPC/cholesterol thin films are shown in Figure 8. At $x \leq 0.3$, dotlike domains are observed on the

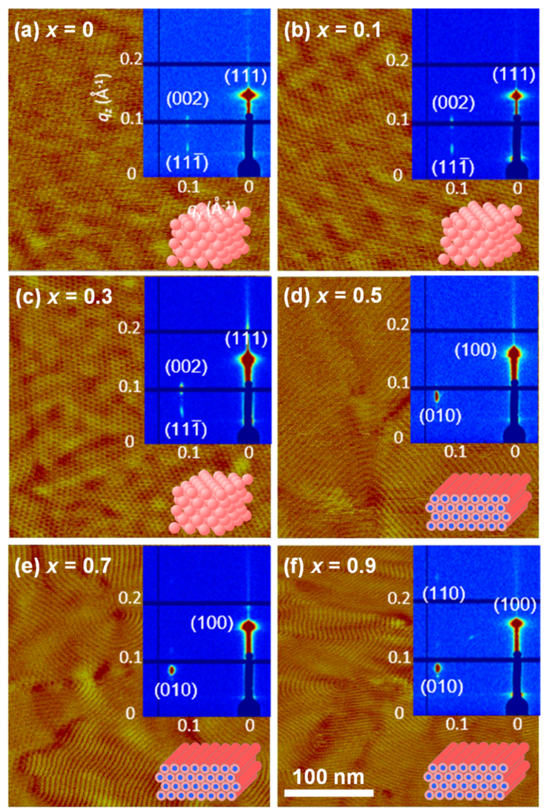

Figure 8. AFM phase images and GISAXS patterns of DOPC/cholesterol thin films at varying x.

surface of the films and the GISAXS data reveal that they are spheres in fcc stacking. At $x \geq 0.5$, the films turn to be fingerprint-like patterns, which are the HEX cylinders parallel to the substrates, as evidenced by the GISAXS data. With one more double bond on the tail, the lamellar structure is absent and only fcc spheres and HEX cylinders can be formed.

DOI: 10.1021/acs.langmuir.8b03075
Langmuir 2019, 35, 3383−3390

The FTIR spectra of the DOPC/cholesterol mixtures in cyclohexane are shown in Figure S2. The absorption band of the phosphate on DOPC red-shifts from 1254 to 1249 cm^{-1} with increasing x, similar to the shift of the phosphate band on egg PC caused by the hydrogen bonding between phosphate and the hydroxyl group on cholesterol. The absorption bands of carbonyl and choline groups, however, are not changed with x, indicating that the flexible unsaturated tails in solutions have more space to accommodate cholesterol so that the DOPC molecular conformation and the distance between adjacent DOPC molecules are unaffected. The FTIR spectra of the DOPC/cholesterol dried films are shown in Figure S3. The absorption band of phosphate in dried films greatly red-shifts from that in solutions and both the bands of phosphate and choline are nearly independent of x, similar to the behaviors of egg PC. Two characteristic bands are found for the carbonyl group, one at 1733 cm^{-1} originating from the closely packed DOPC with stronger dipole−dipole interactions and the other at 1738 cm^{-1} due to weakened interactions. As x increases, the 1738 cm^{-1} band gradually dominates over the 1733 cm^{-1} band, evidencing the insertion of cholesterol to separate DOPC molecules in dried films, also analogous to the trend for egg PC.

Figure 6b displays the DSC thermograms of DOPC/cholesterol mixtures. The T_m of pure DOPC is −6 °C, much lower than that of egg PC (25.5 °C), and the T_m of the mixtures slightly decreases with increasing x. With two unsaturated tails, the configurational regularity of the tails is lower, which hinders the close packing of DOPC to form lamellae at room temperature. DOPC/cholesterol mixtures therefore tend to form fcc spheres or HEX cylinders. Similar to the formation mechanism for egg PC/cholesterol systems, the fcc spheres at $x \leq 0.3$ are kinetically stacked from the original spherical micelles in solutions after solvent evaporation, as evidenced by their slow transformation into HEX cylinders after 5 days shown in Figure S4. The formation of the thermodynamically stable HEX cylinders at $x \geq 0.5$ is due to the insertion of a sufficient amount of cholesterol that enhances the conformational ordering of DOPC tails.[28−31]

DPPC/Cholesterol Mixtures. DPPC bears two saturated tails that tend to closely pack. Following the results of egg PC and DOPC, the DPPC/cholesterol mixtures should prefer to form lamellae. Figure S5 shows the SAXS data of DPPC/cholesterol mixtures. As expected, all the profiles reveal the lamellar structure determined from the q^* and $2q^*$ diffraction peaks. Note that at $x \geq 0.5$, an extra peak appears at $q = 0.18$ $Å^{-1}$, which is the characteristic diffraction of the pure cholesterol crystals (Figure S6). The crystallization of cholesterol at $x = 0.5$ implies that less cholesterol can bind DPPC in comparison to egg PC and DOPC. The excess cholesterol is expelled out of the DPPC lamellae because of the close packing of DPPC. The AFM phase images of the DPPC/cholesterol films shown in Figure S7 are all featureless, and the corresponding GISAXS patterns reveal that all the lamellae are parallel to the substrate (Figure S8). It is interesting that the FTIR spectra of the phosphate on DPPC in dried films are different from those of egg PC and DOPC, as shown in Figure 9. The absorption band of the phosphate on pure DPPC is at 1242 cm^{-1}, indicating a weaker intermolecular interaction between adjacent DPPC headgroups compared to those of egg PC and DOPC (1236−1237 cm^{-1}). This is possibly because the close packing of the saturated tails in expense of the interactions between the headgroups can achieve the minimal free energy. The phosphate band red-shifts to 1232 cm^{-1} at $x \geq 0.5$, indicating that the insertion of cholesterol can interfere with the packing of the tails and allow the headgroups to rearrange to strengthen the interactions. The absorption bands of carbonyl and choline groups are not sensitive to x, possibly due to less cholesterol that inserts into DPPC. As shown in the DSC thermograms of Figure 6c, the T_m of pure DPPC is 64 °C and decreases with increasing x but still higher than the room temperature even at $x = 0.9$. Without double bond on tails, the regular tails on DPPC can crystallize at room temperature for all the ratios, which explains why the lamella is the dominant structure over others.

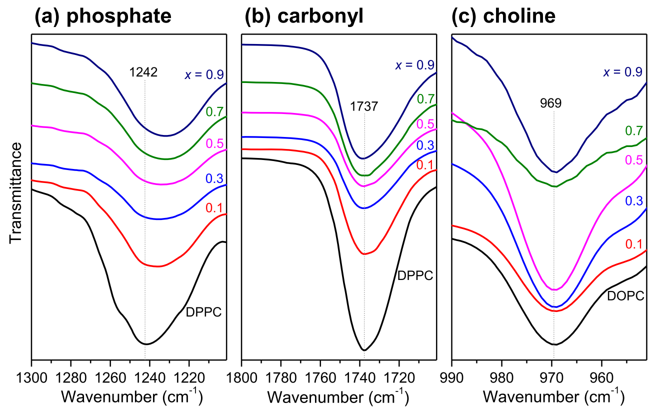

Figure 9. FTIR absorption bands of (a) phosphate, (b) carbonyl, and (c) choline group on DPPC at varying x in dried films at 25 °C.

CONCLUSIONS

We demonstrate in this study that simply mixing two biomolecules, PC and cholesterol, can create a variety of ordered nanostructures in bulk samples or thin films, including lamella, fcc spheres, and HEX cylinders. Remarkably, the scale of the structure is rather small, ∼4−6 nm for the d-spacing and ∼2−3 nm for the domain size. The high incompatibility between the hydrophilic headgroup and the hydrophobic tails of PCs causes the microphase separation even though the molecular weights of the PCs are rather low. We find that the conformation and flexibility of the tails on PCs are key to the formation of the various structures, which can be tuned by the use of PCs with different numbers of double bonds on the tails or by the binding of different amounts of cholesterol to PCs. Such small ordered microdomains formed by the biomolecules are potential for the applications ranging from nanotemplating to biotechnological devices. The systems can also serve as platforms to study the interplays between cholesterol and PCs, which is crucial in cell physiology.

ASSOCIATED CONTENT

Supporting Information

The Supporting Information is available free of charge on the ACS Publications website at DOI: 10.1021/acs.langmuir.8b03075.

Additional FTIR, SAXS, GISAXS, and AFM data (PDF)

AUTHOR INFORMATION

Corresponding Author

*E-mail: shtung@ntu.edu.tw.

ORCID

Shih-Huang Tung: 0000-0002-6787-4955

Notes

The authors declare no competing financial interest.

ACKNOWLEDGMENTS

This work was financially supported by the "Advanced Research Center of Green Materials Science and Technology" from the Featured Area Research Center Program within the framework of the Higher Education Sprout Project by the Ministry of Education (107L9006) and the Ministry of Science and Technology in Taiwan (MOST 103-2221-E-002-186-MY3, 107-3017-F-002-001, and 107-2622-8-006-015). The authors also acknowledge National Synchrotron Radiation Research Center, Taiwan, for facilitating the X-ray scattering experiments.

REFERENCES

(1) Tu, Y.; Peng, F.; Adawy, A.; Men, Y.; Abdelmohsen, L. K. E. A.; Wilson, D. A. Mimicking the Cell: Bio-Inspired Functions of Supramolecular Assemblies. *Chem. Rev.* **2016**, *116*, 2023−2078.

(2) Walde, P.; Giuliani, A. M.; Boicelli, C. A.; Luisi, P. L. Phospholipid-Based Reverse Micelles. *Chem. Phys. Lipids* **1990**, *53*, 265−288.

(3) Scartazzini, R.; Luisi, P. L. Organogels from Lecithins. *J. Phys. Chem.* **1988**, *92*, 829−833.

(4) Shchipunov, Y. A. Lecithin organogel. *Colloids Surf., A* **2001**, *183−185*, 541−554.

(5) Tung, S.-H.; Huang, Y.-E.; Raghavan, S. R. A New Reverse Wormlike Micellar System: Mixtures of Bile Salt and Lecithin in Organic Liquids. *J. Am. Chem. Soc.* **2006**, *128*, 5751−5756.

(6) Tung, S.-H.; Lee, H.-Y.; Raghavan, S. R. A Facile Route for Creating "Reverse" Vesicles: Insights into "Reverse" Self-Assembly in Organic Liquids. *J. Am. Chem. Soc.* **2008**, *130*, 8813−8817.

(7) Leal, C.; Bouxsein, N. F.; Ewert, K. K.; Safinya, C. R. Highly Efficient Gene Silencing Activity of siRNA Embedded in a Nanostructured Gyroid Cubic Lipid Matrix. *J. Am. Chem. Soc.* **2010**, *132*, 16841−16847.

(8) Kim, H.; Leal, C. Cuboplexes: Topologically Active siRNA Delivery. *ACS Nano* **2015**, *9*, 10214−10226.

(9) Kang, M.; Leal, C. Soft Nanostructured Films for Actuated Surface-Based siRNA Delivery. *Adv. Funct. Mater.* **2016**, *26*, 5610−5620.

(10) Phang, T.-L.; Franses, E. I. Physically Self-Assembled Monolayers (PSAMs) of Lecithin Lipids at Hydrophilic Silicon Oxide Interfaces. *Langmuir* **2006**, *22*, 1609−1618.

(11) Rittman, M.; Amenitsch, H.; Rappolt, M.; Sartori, B.; O'Driscoll, B. M. D.; Squires, A. M. Control and Analysis of Oriented Thin Films of Lipid Inverse Bicontinuous Cubic Phases Using Grazing Incidence Small-Angle X-ray Scattering. *Langmuir* **2013**, *29*, 9874−9880.

(12) Wadsäter, M.; Barauskas, J.; Nylander, T.; Tiberg, F. Nonlamellar Lipid Liquid Crystalline Model Surfaces for Biofunctional Studies. *Soft Matter* **2013**, *9*, 8815−8819.

(13) Gupta, G.; Iyer, S.; Leasure, K.; Virdone, N.; Dattelbaum, A. M.; Atanassov, P. B.; López, G. P. Stable and Fluid Multilayer Phospholipid-Silica Thin Films: Mimicking Active Multi-lamellar Biological Assemblies. *ACS Nano* **2013**, *7*, 5300−5307.

(14) Kang, M.; Tuteja, M.; Centrone, A.; Topgaard, D.; Leal, C. Nanostructured Lipid-Based Films for Substrate-Mediated Applications in Biotechnology. *Adv. Funct. Mater.* **2018**, *28*, 1704356.

(15) Steer, D.; Kang, M.; Leal, C. Soft Nanostructured Films for Directing the Assembly of Functional Materials. *Nanotechnology* **2017**, *28*, 142001.

(16) Leibler, L. Theory of Microphase Separation in Block Copolymers. *Macromolecules* **1980**, *13*, 1602−1617.

(17) Bates, F.; Fredrickson, G. H. Block Copolymer Thermodynamics: Theory And Experiment. *Annu. Rev. Phys. Chem.* **1990**, *41*, 525−557.

(18) Cushen, J. D.; Otsuka, I.; Bates, C. M.; Halila, S.; Fort, S.; Rochas, C.; Easley, J. A.; Rausch, E. L.; Thio, A.; Borsali, R.; Willson, C. G.; Ellison, C. J. Oligosaccharide/Silicon-Containing Block Copolymers with 5 nm Features for Lithographic Applications. *ACS Nano* **2012**, *6*, 3424−3433.

(19) Pitet, L. M.; Wuister, S. F.; Peeters, E.; Kramer, E. J.; Hawker, C. J.; Meijer, E. W. Well-Organized Dense Arrays of Nanodomains in Thin Films of Poly(dimethylsiloxane)-b-poly(lactide) Diblock Copolymers. *Macromolecules* **2013**, *46*, 8289−8295.

(20) Luo, Y.; Montarnal, D.; Kim, S.; Shi, W.; Barteau, K. P.; Pester, C. W.; Hustad, P. D.; Christianson, M. D.; Fredrickson, G. H.; Kramer, E. J.; Hawker, C. J. Poly(dimethylsiloxane-b-methyl methacrylate): A Promising Candidate for Sub-10 nm Patterning. *Macromolecules* **2015**, *48*, 3422−3430.

(21) Kwak, J.; Mishra, A. K.; Lee, J.; Lee, K. S.; Choi, C.; Maiti, S.; Kim, M.; Kim, J. K. Fabrication of Sub-3 nm Feature Size Based on Block Copolymer Self-Assembly for Next-Generation Nanolithography. *Macromolecules* **2017**, *50*, 6813−6818.

(22) Nowak, S. R.; Hwang, W.; Sita, L. R. Dynamic Sub-10-nm Nanostructured Ultrathin Films of Sugar-Polyolefin Conjugates Thermoresponsive at Physiological Temperatures. *J. Am. Chem. Soc.* **2017**, *139*, 5281−5284.

(23) Nickmans, K.; Murphy, J. N.; de Waal, B.; Leclère, P.; Doise, J.; Gronheid, R.; Broer, D. J.; Schenning, A. P. H. J. Sub-5 nm Patterning by Directed Self-Assembly of Oligo(Dimethylsiloxane) Liquid Crystal Thin Films. *Adv. Mater.* **2016**, *28*, 10068−10072.

(24) Nickmans, K.; Schenning, A. P. H. J. Directed Self-Assembly of Liquid-Crystalline Molecular Building Blocks for Sub-5 nm Nanopatterning. *Adv. Mater.* **2018**, *30*, 1703713.

(25) Yu, X.; Yue, K.; Hsieh, I.-F.; Li, Y.; Dong, X.-H.; Liu, C.; Xin, Y.; Wang, H.-F.; Shi, A.-C.; Newkome, G. R.; Ho, R.-M.; Chen, E.-Q.; Zhang, W.-B.; Cheng, S. Z. D. Giant Surfactants Provide a Versatile Platform for Sub-10-nm Nanostructure Engineering. *Proc. Natl. Acad. Sci. U.S.A.* **2013**, *110*, 10078−10083.

(26) Huang, M.; Hsu, C.-H.; Wang, J.; Mei, S.; Dong, X.; Li, Y.; Li, M.; Liu, H.; Zhang, W.; Aida, T.; Zhang, W.-B.; Yue, K.; Cheng, S. Z. D. Selective Assemblies of Giant Tetrahedra via Precisely Controlled Positional Interactions. *Science* **2015**, *348*, 424−428.

(27) Sackmann, E. Biological Membranes Architecture and Function. In *Structure and Dynamics of Membranes*, 1st ed.; Lipowsky, R., Sackmann, E., Eds.; Elsevier: North Holland, 1995; Vol. *1A*, pp 1−62.

(28) Robinson, A. J.; Richards, W. G.; Thomas, P. J.; Hann, M. M. Behavior of Cholesterol and Its Effect on Head Group and Chain Conformations in Lipid Bilayers: A Molecular Dynamics Study. *Biophys. J.* **1995**, *68*, 164−170.

(29) Hung, W.-C.; Lee, M.-T.; Chen, F.-Y.; Huang, H. W. The Condensing Effect of Cholesterol in Lipid Bilayers. *Biophys. J.* **2007**, *92*, 3960−3967.

(30) de Meyer, F.; Smit, B. Effect of Cholesterol on the Structure of a Phospholipid Bilayer. *Proc. Natl. Acad. Sci. U.S.A.* **2009**, *106*, 3654−3658.

(31) Chong, P. L. Evidence for Regular Distribution of Sterols in Liquid Crystalline Phosphatidylcholine Bilayers. *Proc. Natl. Acad. Sci. U.S.A.* **1994**, *91*, 10069−10073.

(32) Zull, J. E.; Greanoff, S.; Adam, H. K. Interaction of Egg Lecithin with Cholesterol in the Solid State. *Biochemistry* **1968**, *7*, 4172−4176.

(33) Ohvo-Rekilä, H.; Ramstedt, B.; Leppimäki, P.; Slotte, J. P. Cholesterol interactions with phospholipids in membranes. *Prog. Lipid Res.* **2002**, *41*, 66−97.

(34) Jeng, U.-S.; Su, C. H.; Su, C.-J.; Liao, K.-F.; Chuang, W.-T.; Lai, Y.-H.; Chang, J.-W.; Chen, Y.-J.; Huang, Y.-S.; Lee, M.-T.; Yu, K.-L.; Lin, J.-M.; Liu, D.-G.; Chang, C.-F.; Liu, C.-Y.; Chang, C.-H.; Liang, K. S. A small/wide-angle X-ray scattering instrument for structural characterization of air-liquid interfaces, thin films and bulk specimens. *J. Appl. Crystallogr.* **2010**, *43*, 110−121.

(35) Förster, S.; Timmann, A.; Konrad, M.; Schellbach, C.; Meyer, A.; Funari, S. S.; Mulvaney, P.; Knott, R. Scattering Curves of Ordered Mesoscopic Materials. *J. Phys. Chem. B* **2005**, *109*, 1347−1360.
(36) Njauw, C.-W.; Cheng, C.-Y.; Ivanov, V. A.; Khokhlov, A. R.; Tung, S.-H. Molecular Interactions between Lecithin and Bile Salts/Acids in Oils and Their Effects on Reverse Micellization. *Langmuir* **2013**, *29*, 3879−3888.
(37) Lin, S.-T.; Lin, C.-S.; Chang, Y.-Y.; Whitten, A. E.; Sokolova, A.; Wu, C.-M.; Ivanov, V. A.; Khokhlov, A. R.; Tung, S.-H. Effects of Alkali Cations and Halide Anions on the Self-Assembly of Phosphatidylcholine in Oils. *Langmuir* **2016**, *32*, 12166−12174.
(38) Hauser, H.; Pascher, I.; Pearson, R. H.; Sundell, S. Preferred Conformation and Molecular Packing of Phosphatidylethanolamine and Phosphatidylcholine. *Biochim. Biophys. Acta* **1981**, *650*, 21−51.

DOI: 10.1021/acs.langmuir.8b03075
Langmuir 2019, 35, 3383−3390